Vehicle sideslip estimation: A kinematic based approach ☆

Donald Selmanaj[a,*], Matteo Corno, Giulio Panzani and Sergio M. Savaresi[b]

[a] *Department of Automation, Polytechnic University of Tirana, Sheshi "Nënë Tereza", Nr.4, Tirana, Albania.*
[b] *Dipartimento di Elettronica, Informazione e Bioingegneria, Politecnico di Milano, Piazza L. da Vinci, 32, 20133, Milano, Italy.*

Abstract

This paper deals with vehicle sideslip angle estimation. The paper introduces an industrially amenable kinematic-based approach that does not need tire-road friction parameters or other dynamical properties of the vehicle. The convergence of the estimate is improved by the introduction of a heuristic based on readily available inertial measurements. The method is tested on a vast collection of tests performed in different conditions, showing a satisfactory behavior despite not using any information on the road friction. The extensive experimental validation confirms that the estimate is robust to a wide range of driving scenarios.

Keywords: automotive estimation, sideslip angle estimation, model free estimation, four-wheeled vehicles, vehicle stability control.

1. Introduction

Over the last few decades, industrial and academic research has dedicated great effort towards safer and better performing four-wheeled vehicles. Sensors and actuators evolution ([1, 2]) has made possible the use of advanced control techniques acting on vehicle dynamics with the aim of generating suitable yaw moment to avoid dangerous conditions or increase performances. Nowadays electronic stability control (ESC) is a standard technology in almost all commercial passenger cars ([3, 4]), while researchers continue to explore the possibility of using rear axle steering to improve the vehicle stability ([5, 6]). From a control standpoint, besides the problem of defining the control laws, the knowledge/measurement of vehicle states presents a challenge.

From the vehicle stability standpoint, the most important states are sideslip angle, *i.e.* the angle between the vehicle longitudinal axis and the direction

☆ The content of this paper has been patented (WO2014EP72439).

* Corresponding author
Email address: donald.selmanaj@fie.upt.al (Donald Selmanaj)

of the vehicle velocity, and the sideslip rate. These are used to determine the control action, re-schedule the parameters of the control architecture or re-establish the vehicle stability. To these ends the fast and road-independent estimation of the two quantities is crucial, [7, 8].

The sideslip angle and its rate can be measured via optical sensors or GPS with sufficient accuracy in all road conditions; however these solutions are prohibitively expensive for commercial cars (optical sensors) or lack reliability (GPS). Methods for integrating inertial measurements with low-cost GPS measurements ([9, 10, 11, 12, 13, 14], for example) or tire force sensors ([15, 16], for example) have been proposed. However, GPS is not present in all commercial vehicles and tire force sensors introduce excessive costs and complexity to the vehicle design [17, 18]. Therefore, online estimation techniques using low-cost inertial sensors have been widely studied in the automotive research. The proposed method exploits low cost off-the-shelf measurements, *i.e.* vehicle accelerations along the three axis, vehicle angular rates, wheel angular rates and wheel steering angle.

In the realm of methods using standard measurements, there exist two main families of approaches: black-box or white-box estimation. Black-box approaches derive methods that directly estimate the sideslip angle from the measurements. Assuming the sideslip angle as a nonlinear function of the yaw rate and the lateral acceleration, a neural network can model the vehicle behavior and can be used to estimate the sideslip angle, [19]. The main drawback of the method is that it does not consider the relation with the vehicle speed. A similar method is used in [20]. The authors propose a nonlinear estimator, designed based on the direct virtual sensor approach. A neural network exploits the lateral acceleration, steering angle, yaw rate and longitudinal velocity measurements and forms the core of the estimator. Despite showing promising performance, both papers do not consider the effect of road friction in the analysis. Varying road conditions could affect the estimation accuracy. These are data driven approaches; if the training set has not considered a particular type of ground, there is no way of guaranteeing how the estimator will behave when driving on such roads.

For these reason, most solutions include model-based estimation techniques. An important aspect classifying these methods is the vehicle model type; two main categories can be identified: dynamic model-based and kinematic model-based methods.

Dynamic models provide a good description of the vehicle lateral dynamics, but require a good knowledge of the vehicle parameters, specially tire-road interaction conditions. As a matter of fact, the tire friction model and its online estimation plays a key role in many studies. A sliding mode observer, with a simplified tire model, is proposed in [21], and is shown to have good results with lateral acceleration not exceeding 0.6 g (*i.e.*, linear region). In [22], the authors present a two-step method: the first step includes a sliding mode observer that provides the tire-road forces while in the second step an Extended Kalman Filter (EKF) estimates the sideslip angle and the cornering stiffness. [23] presents a dual EKF method. Two filters run in parallel, one dedicated to

the estimation of the vehicle state while the others estimates. Alternative solutions relying on the EKF are presented in [24], where a decision tree classifies the uncertainties and disturbances to assist an EKF, and in [25], where the vehicle state and the tire-road forces are reconstructed. A critical point of dynamic model-based methods is the difficulty of estimating the tire friction. This task requires exciting running conditions, which are not always verified. Indeed, the aforementioned methods are validated on exciting maneuvers and lack extensive analysis during low excitation tests. Furthermore, dynamic models lose their reliability on high acceleration conditions where the vehicle dynamics becomes nonlinear, mainly due to tires behavior. Experimental results of aforementioned solutions present limited lateral accelerations (0.6 g). Other disadvantages regarding these methods concern the vehicle mass and yaw inertia sensitivity; both parameters can experience large variations.

An alternative approach are kinematic model-based methods, which rely on a simple vehicle model that correlates the vehicle longitudinal and lateral velocities with longitudinal and lateral accelerations and the yaw rate. These methods do not depend on vehicle or tire friction parameters. A well known nonlinear vehicle state observer was introduced in [26] and proved to be asymptotically stable for all cornering conditions (non-zero yaw rate). In [27], the authors strengthen the aforementioned method proposing an online offset estimation via a recursive identification approach. An EKF designed on the kinematic model is presented in [28]; the effectiveness of the method is shown on short maneuvers (10 s). Based on the same model, in [29] the authors propose a sliding mode observer; the observer is tested and analyzed on a simulation environment and a double lane change maneuver. According to the best of our knowledge and literature research, these are the only studies relying on a pure kinematic model and are all analyzed on simulation data or short duration experiments. All results evidence that kinematic model-based methods are reliable for transient maneuvers, but they suffer from estimation errors on nearly steady-state conditions.

One option for overcoming these limits is to design observers that join the advantages of the kinematic and dynamic model. The method proposed in [30] relies on the kinematic formulation during transient maneuvers and on a state observer, designed on the single track model, on nearly steady-state maneuvers. During transient maneuvers the kinematic estimate is used to update the friction parameters of the single track model. Experimental results prove the validity of the method. In [31], a feedback algorithm is fed with the side force estimated from the lateral acceleration and the side force given by a tire model with an online estimate of the road friction coefficient. Other methods mixing the two approaches are shown in [32] and [33]. Both studies combine a kinematic model and a bicycle model with online friction adaption through a weighted mean; experimental results for the standard double lane change maneuver are shown. In [34], the authors present a method based on a nonlinear observer. The method joins a kinematic model with a correction term computed on a friction model which is estimated online. In [35, 36] an online road banking estimation is added and the results are compared with an EKF. The proposed approach is tested on different experimental tests. However, exciting running

conditions (*i.e.*, varied driving path) are essential for the stability of the method and solutions for particular driving conditions have been found.

Although different architectures can be used to combine the kinematic and the dynamic model, [37], and some studies show good results on standard maneuvers, the excitation of the driving conditions remains a major limitation. Especially on strong curves following long straight drivings (*i.e.*, when the friction estimation can not be updated) and when the friction experiences step variations during curves, methods relying on the friction estimation are more prone to sideslip estimation errors. The present work aims to give a reliable solution to the sideslip angle estimation problem without the need of estimating the friction parameters and is based on the kinematic approach. First, the observer proposed in [26] is modified to overcome the unobservability for zero yaw rate conditions without using the dynamical model (or road parameters); the method relies on a heuristic that drives the sideslip angle estimation to zero when the vehicle is moving straight. The heuristic is computed as a static function of the inertial measurements. Therefore, a method for the online offset estimation and one for the vehicle longitudinal speed estimation are proposed. The validity and reliability of the method is shown on several realistic driving tests representing hours worth of driving. These tests include highly dynamic and nearly steady state maneuvers. To the best of the authors knowledge this paper represents the most thorough experimental validation of a sideslip angle estimation available in the open scientific literature. Results on different road conditions demonstrate the robustness of the method to varying road conditions. The method and the equations are described in continuous time. However, to obtain the experimental results, the method has been implemented on an off-the-shelf electronic control unit runnning at 100 Hz.

The paper is organized as follows. In Section 2 the kinematic observer and the longitudinal vehicle speed estimation are described. Section 3 describes the structure of the estimation method including the kinematic observer, the offset estimation, the roll angle estimation and the undesired effects compensation. In Section 4, the offset estimation algorithm is presented. In Sections 5 and 6, experimental results are shown and sensitivity to vehicle mass and road surface is analyzed. The paper ends with some concluding remarks. Part of the present work is protected by the patent [38].

2. Kinematic model-based observer

The vehicle state observer is based on the kinematic model shown in (1), and quantities refer to the schematic of Figure 1. The model relates the vehicle accelerations (A_x and A_y) to the vehicle velocities derivatives ($\dot{V}_x$ and $\dot{V}_y$) and the yaw rate (ω_z). For straight movement, the vehicle accelerations correspond to the vehicle velocities derivatives. As the vehicle turns, the longitudinal acceleration is influenced by the lateral velocity (V_y) and the yaw rate while the lateral acceleration is influenced by the longitudinal velocity (V_x) and the yaw rate.

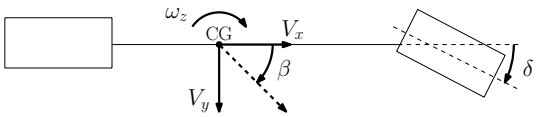

Figure 1: Single track model. δ is the front wheels steer.

$$\begin{cases} A_x(t) = \dot{V}_x(t) - \omega_z(t) V_y(t) \\ A_y(t) = \dot{V}_y(t) + \omega_z(t) V_x(t). \end{cases} \tag{1}$$

Equation (1) can be rewritten as a Linear Parameter Varying system, where the vehicle velocities represent the system state vector, the yaw rate is considered to be a time varying parameter and the vehicle accelerations are considered as inputs:

$$\begin{aligned} \begin{bmatrix} \dot{V}_x(t) \\ \dot{V}_y(t) \end{bmatrix} &= \underbrace{\begin{bmatrix} 0 & \omega_z(t) \\ -\omega_z(t) & 0 \end{bmatrix}}_{[A]} \begin{bmatrix} V_x(t) \\ V_y(t) \end{bmatrix} + \underbrace{\begin{bmatrix} 1 & 0 \\ 0 & 1 \end{bmatrix}}_{[B]} \begin{bmatrix} A_x(t) \\ A_y(t) \end{bmatrix} \\ y(t) &= \underbrace{\begin{bmatrix} 1 & 0 \end{bmatrix}}_{[C]} \begin{bmatrix} V_x(t) \\ V_y(t) \end{bmatrix}. \end{aligned} \tag{2}$$

The longitudinal velocity is considered as the output variable and is used as the comparison quantity for the state feedback observer. The sideslip angle is computed as:

$$\beta(t) = \arctan\left(\frac{V_y(t)}{V_x(t)}\right). \tag{3}$$

Based on this model, the following nonlinear state observer was first introduced in [26]:

$$\begin{bmatrix} \dot{\hat{V}}_x(t) \\ \dot{\hat{V}}_y(t) \end{bmatrix} = (A - KC) \begin{bmatrix} \hat{V}_x(t) \\ \hat{V}_y(t) \end{bmatrix} + B \begin{bmatrix} A_x(t) \\ A_y(t) \end{bmatrix} + KV_x, \tag{4}$$

where K, the observer gain matrix, was defined as:

$$K = \begin{bmatrix} 2\alpha |\omega_z(t)| & \left(\alpha^2 - 1\right) \omega_z(t) \end{bmatrix}^T.$$

The observer is based on two contributions: the vehicle behavior, reproduced according to the kinematic model and the feedback correction of the longitudinal velocity measure derived from the wheel velocities. While the stability during cornering has been proved by the authors in [26], two main issues remain:

1. Longitudinal velocity is updated only on cornering, although on straight maneuvers the reliability of the velocity measure through wheel angular velocities is higher.
2. For straight maneuvers the observability of (2) is lost. In these conditions, the observer trivially integrates the accelerations. Small measurement offsets and errors combined with long straight maneuvers, which are common, can cause the filter divergence.

The main innovation introduced here regards the kinematic model, (2); it expresses the behavior of a free body accelerated on a plane and includes lateral drift conditions with zero yaw rate. However, it is extremely unlikely for a four-wheel vehicle to drift laterally without rotating on its vertical axis. Moreover, sideslip angle estimators usually are part of an electronic stability control package designed to specifically avoid getting in those conditions. In other words, it is extremely unlikely for the sideslip angle to be different from zero if the vehicle is moving straight. This information can be accounted for by adding a stabilizing term $(-F(t)\,V_y(t))$ in the second equation of (2). Choosing $F(t) > 0$ and sufficiently high when the vehicle is moving straight, the lateral velocity (and thus the sideslip angle) is forced to converge to zero since on straight driving A_y and ω_z are nearly zero. Accordingly, $F(t)$ is scheduled by a heuristic that identifies straight driving.

The observer expression is given in (5); it is derived from the one presented in [26], introducing two major novelties to cope with the aforementioned issues. The observer state consists of the vehicle longitudinal and lateral velocity, the acceleration measures are considered as inputs and the yaw rate is considered as a measurable time-varying parameter.

$$\begin{aligned}\begin{bmatrix}\dot{\hat{V}}_x(t)\\ \dot{\hat{V}}_y(t)\end{bmatrix} = &\underbrace{\begin{bmatrix}-\alpha_0-\alpha_1|\omega_z(t)| & \omega_z(t)\\ -(\alpha_2+1)\,\omega_z(t) & -F(t)\end{bmatrix}}_{[A-K_n(\omega_z)C]}\begin{bmatrix}\hat{V}_x(t)\\ \hat{V}_y(t)\end{bmatrix}\\ &+\underbrace{\begin{bmatrix}1 & 0\\ 0 & 1\end{bmatrix}}_{[B]}\begin{bmatrix}A_x(t)\\ A_y(t)\end{bmatrix}+\underbrace{\begin{bmatrix}\alpha_0+\alpha_1|\omega_z(t)|\\ \alpha_2\omega_z(t)\end{bmatrix}}_{[K_n(\omega_z)]}V_x\end{aligned} \tag{5}$$

The gain matrix $K_n(\omega_z)$ is composed of yaw rate dependent and constant terms. $\alpha_1|\omega_z|$ and $\alpha_2\omega_z$ update the observer state on cornering, while α_0 guarantees the $\hat{V}_x$ update also on straight maneuvers. V_x is the vehicle longitudinal velocity and is obtained from the equivalent linear wheel velocity, as described in Section 2.3. In accordance with the reasoning on the straight driving, the term $F(t)$ is added in order to drive the sideslip angle to zero.
In principle, the behavior of the observer is the following: (i) if F is small (i.e., close to 0) the vehicle state is estimated from the kinematic model dynamics and the V_x measurement; (ii) if F is large the estimated lateral velocity is driven to a small value, while the longitudinal velocity is updated by V_x. A proper modulation of F is proposed in Section 2.1.

2.1. Heuristic scheduling

The main function of the heuristic is to merge the kinematic model with empirical information. F determines the strength of the stabilizing effect; it needs to be carefully weighted to make sure it intervenes only when needed. Figure 2 proposes the F scheduling block diagram, where δ is the steering wheel

angle and $\dot{\beta}$ is the sideslip angle derivative, given by (6).

$$\dot{\beta}(t) = \frac{A_y(t) - \omega_z(t) V_x(t)}{V_x(t)}. \tag{6}$$

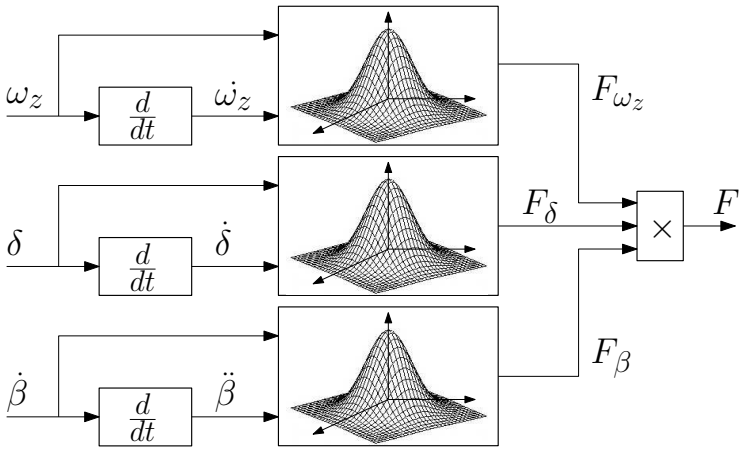

Figure 2: Heuristic dynamics computation.

The scheduling of F is based on the idea that, as the vehicle curves, the kinematic model is observable and the closed loop observer performs correctly; on the other hand, during straights driving, F should be large to drive the sideslip estimation to zero. Therefore measurements used to schedule F are cornering indicators. $\dot{\beta}$ and ω_z are clear indicators of cornering maneuvers. However, maneuvers on low grip roads and maneuvers close to pure drift can present small yaw rate values, while nearly steady-state maneuvers can present small $\dot{\beta}$. For these maneuvers, the steering angle is highly informative in discerning straight driving from cornering.
F_{ω_z}, F_δ and F_β behave as follows: (i) if ω_z or $\dot{\omega}_z$ is different from zero F_{ω_z} is driven to zero; (ii) if δ or $\dot{\delta}$ is different from zero F_δ is driven to zero and (iii) if $\dot{\beta}$ or $\ddot{\beta}$ is different from zero F_β is driven to zero. If one of the three terms composing F is set to zero, F is zero. F_{ω_z},F_δ and F_β smoothly vary from zero to a maximum value and can be computed through static maps or mathematical expressions. Using mathematical expressions with few parameters, however, reduces the tuning effort. The expression computing the three terms of F (F_{ω_z}, F_δ and F_β) is the bivariate Gaussian Distribution:

$$F_i = e^{-\frac{1}{2}\left(\frac{i^2}{\sigma_i^2} + \frac{di^2}{\sigma_{di}^2}\right)} \quad i = \omega_z, \delta, \dot{\beta}. \tag{7}$$

One advantage of expression (7) is its easy tuning. For each measurement and derivative involved, only one parameter determines the influence on F. Moreover,
180 the Gaussian shape guarantees an insensitive region on the top of the bell,

that is when the corresponding measurement is zero. More in details, for each variable and its related derivative, the corresponding parameter (σ_i and σ_{di}) indicates the vehicle conditions in which the observer output is driven towards zero. Ideally, this should happen only when the mentioned variables are close to zero (the sideslip angle is not observable). However, care must be paid no to classify measurement noise as vehicle motion; the amplitude of the bell provides a tuning for this aspect. Thus a good starting guess for parameters tuning comes from the amplitude of the noise of the corresponding signal: the width of each bell should be large enough such that the variations of F due to measurement noises is negligible. The bell can be then further increased to "activate" the kinematic observer only during highly dynamic maneuvers. The derivatives of the signals are computed by derivative filters with a cutoff frequency of 10 Hz. The filters are designed in continuous time and converted in discrete time through the Euler forward method. The sampling frequency (100 Hz) and the cutoff frequency are such that the discretization process does not produce any relevant deviation from the continuous time form. The filters combined with the shape of the gaussian distribution cancel the effect of measurements noise.

2.2. Stability analysis

The error dynamics of the proposed kinematic model-based observer (5) are given by:

$$\begin{bmatrix} \dot{e_x} \\ \dot{e_y} \end{bmatrix} = \begin{bmatrix} \dot{V}_x - \dot{\hat{V}}_x \\ \dot{V}_y - \dot{\hat{V}}_y \end{bmatrix} = \begin{bmatrix} -\alpha_0 - \alpha_1 \left|\omega_z\right| & \omega_z \\ -\left(\alpha_2 + 1\right)\omega_z & -F \end{bmatrix} \begin{bmatrix} e_x \\ e_y \end{bmatrix} + \begin{bmatrix} 0 \\ F \end{bmatrix} V_y. \tag{8}$$

The latter is a non-autonomous system and the vehicle lateral speed (V_y) plays the role of the external excitation. Given the heuristic nature of F, the analytic stability of (8) is performed with a simplified, yet insightful, procedure, distinguishing three running conditions:

1. *During curves,* the heuristic F is driven to zero and (8) reduces to an autonomous system. The stability of the reduced system can be analyzed using the following Lyapunov function:

$$V\left(\begin{bmatrix} e_x \\ e_y \end{bmatrix}\right) = \frac{\left(\alpha_2 + 1\right) e_x^2 + e_y^2}{2}. \tag{9}$$

   Combining equation (9) and (8) with $F \approx 0$, one can obtain the following Lypunov function derivative:

$$\dot{V}\left(\begin{bmatrix} e_x \\ e_y \end{bmatrix}\right) = -\left(\alpha_2 + 1\right)\left(\alpha_0 + \alpha_1 \left|\omega_z\right|\right) e_x^2. \tag{10}$$

   Therefore, choosing $\alpha_0, \alpha_1, \alpha_2 > 0$, on curve the new observer (5) presents similar stability behavior of the original observer (4).

2. *During straight driving,* (8) reduces again to an autonomous system, since $\omega_z \approx 0$ and $V_y \approx 0$. In these conditions α_0 and F determine the convergence speed of the system to $\hat{V_x} \approx V_x$ and $\hat{V_y} \approx 0$.

3. *During the transition from a corner to straight driving and viceversa,* both F and V_y are different from zero and the exogenous input influences the error dynamics. Since V_y is limited (*i.e.*, physical quantity) and F is limited by construction, the estimation error is limited. If the corner in and out are short the influence of the exogenous term is negligible. Although the latter claim is not proven formally, the extensive experimental results shown in Section 5 evidence that these conditions do not cause any instability and do not deteriorate the estimate.

2.3. Longitudinal velocity estimation

The vehicle longitudinal velocity measurement (V_x) is essential for the vehicle state observer (5). However, the longitudinal velocity is difficult to measure directly and has to be derived from the wheel velocities. Considering a constant wheel radius the equivalent linear wheel velocities (V_{FL}, V_{FR}, V_{RL}, V_{RR}) are trivially obtained from the wheel rotational velocity measurements. Although wheel velocity measurements represent a reliable source of information, they have to be properly processed to mitigate undesired effects. In [26], the authors do not account for any effect and compute the vehicle longitudinal velocity as the average of the equivalent linear velocity of the wheels. Here we propose a method to compensate the measurement error due to yaw rate, wheel longitudinal slip and steering angle. The method is based on kinematic considerations and does not require any additional sensor. Figure 3 shows the effects influencing the wheel velocities. The front wheel velocities measurements are affected by the front wheel steer angle and the vehicle yaw rate affects all the wheels as they are distant from the vehicle center of mass. All the cited phenomena are

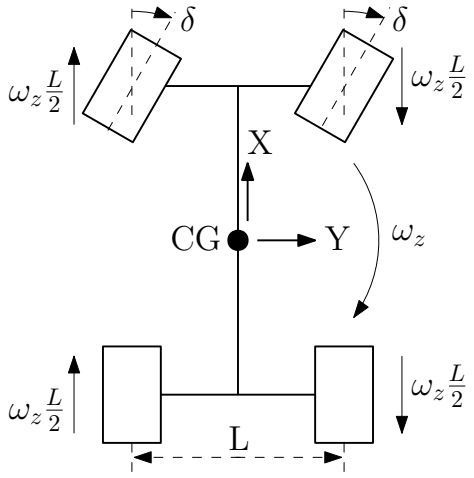

Figure 3: Steer and yaw rate effects on the wheel velocity measurements

compensated as follows:

$$\begin{aligned} V_{FL} = V_{FL}^{meas} cos\delta - \omega_z \frac{L}{2} \quad V_{FR} = V_{FR}^{meas} cos\delta + \omega_z \frac{L}{2} \\ V_{RL} = V_{RL}^{meas} - \omega_z \frac{L}{2} \quad V_{RR} = V_{RR}^{meas} + \omega_z \frac{L}{2}, \end{aligned} \tag{11}$$

where V_{FL}^{meas}, V_{FR}^{meas}, V_{RL}^{meas} and V_{RR}^{meas} are the measured equivalent linear velocities of the wheels and L is the wheel track, assumed equal between front and rear wheels without any loss of generality. Besides the kinematic effects described above, the wheel velocity measurements are affected by longitudinal slip, *i.e.*, the discrepancy between the linear velocity of the wheel center and the linear velocity of the wheel contact point. The longitudinal slip is the cause for the longitudinal force generated by the wheel, [39]. If the wheel is accelerated, the linear wheel velocity at the contact point will be higher than the vehicle velocity and the generated force will be positive (*i.e.*, in the sense that it will accelerate the vehicle). Viceversa, if the wheel is decelerated (braking), the linear wheel velocity at the contact point will be smaller than the vehicle velocity and the generated force will be negative (*i.e.*, it will decelerate the vehicle). To cope with the slip problem and estimate the vehicle slip, in [40] the authors propose an algorithm based on the selection of the best-wheel velocity, *i.e.* the wheel that presents the lower slip. The algorithm relies on the measurement of the wheel torques and requires expensive sensors, not available in commercial cars. Here the estimation is based entirely on kinematic considerations and operates a smooth selection between the wheel velocities. The idea is to identify the lowest slip wheel by exploiting the acceleration of the vehicle and the aforementioned reasoning on the wheel slips. If the vehicle is accelerating, the wheels tend to have higher velocity than the vehicle, thus the lowest wheel velocity is the closest to the vehicle velocity. Viceversa, if the vehicle is decelerating, the wheels tend to have lower velocity and the highest wheel velocity is the closest to the vehicle velocity. Acceleration and deceleration maneuvers are identified through thresholds on the longitudinal acceleration measurement (Figure 4). For nearly zero longitudinal acceleration the vehicle velocity is computed as a

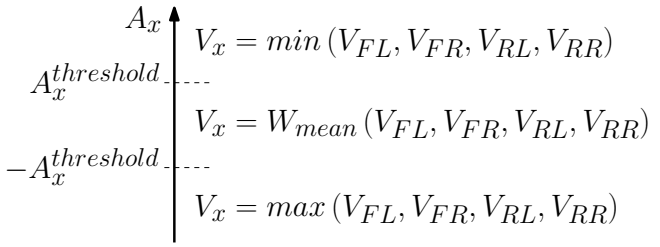

Figure 4: V_x estimation algorithm.

weighted mean of the wheel velocities according to the following equation:

$$W_{mean} = \frac{1}{\sum_i W_i} \sum_i W_i V_i \quad i = FL, FR, RL, RR. \tag{12}$$

For each wheel (V_i), the weight (W_i) indicates the reliability of the wheel velocity measurement and its influence on the estimated velocity. Weights are computed with the following idea: if the derivative of a wheel velocity is different from the measured A_x or the wheel velocity itself is different from the estimated velocity than the weight is driven to zero and the wheel velocity is not considered in the weighted average. A bivariate Gaussian Distribution (Figure 5) computes the weigths:

$$W_i = e^{-\frac{\left(Ax - \frac{dV_i}{dt}\right)^2}{2\cdot\sigma_{w1}^2} - \frac{\left(\hat{V}_x^{t-1} - V_i\right)^2}{2\cdot\sigma_{w2}^2}} \quad i = FL, FR, RL, RR. \tag{13}$$

$\hat{V}_x^{t-1}$ is the estimated vehicle velocity at the previous time step. Since the bandwidth of $\hat{V}_x$ is much lower than the bandwidth of wheel velocities (V_i), considering the vehicle velocity estimated at the previous time step introduces a negligible effect. The weighting algorithm automatically discards the wheels that diverge due to strong braking or acceleration. The derivative of the wheel velocities are computed by real derivative filters with a cutoff frequency of 10 Hz.

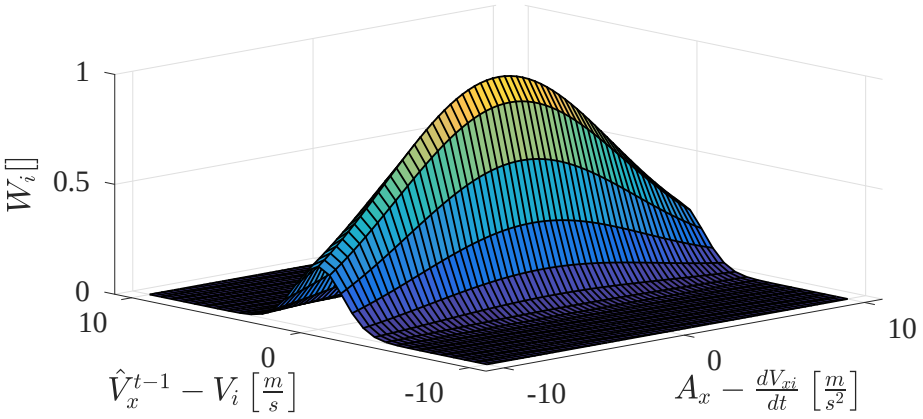

Figure 5: Wheel velocity weight function.

3. Side slip angle estimate: complete observer

The complete observer is shown in Figure 6. The core of the method is the *Vehicle State Observer*, presented in Section 2, that requires the vehicle center of mass (CG) accelerations, the yaw rate and the estimated vehicle longitudinal velocity. It represents the main contribution of the work. The core estimator requires additional blocks to properly process the IMU measurements and avoid undesired effects. Gravity acceleration influences the measurements through the vehicle roll. A roll estimation and gravity compensation algorithm is also included and presented in Section 3.1. An online offset estimation algorithm is presented in Section 4. As the inertial measurement unit (IMU) is not

placed at the center of mass and might be misaligned with the vehicle axes, the measurements are rotated and transferred to CG.

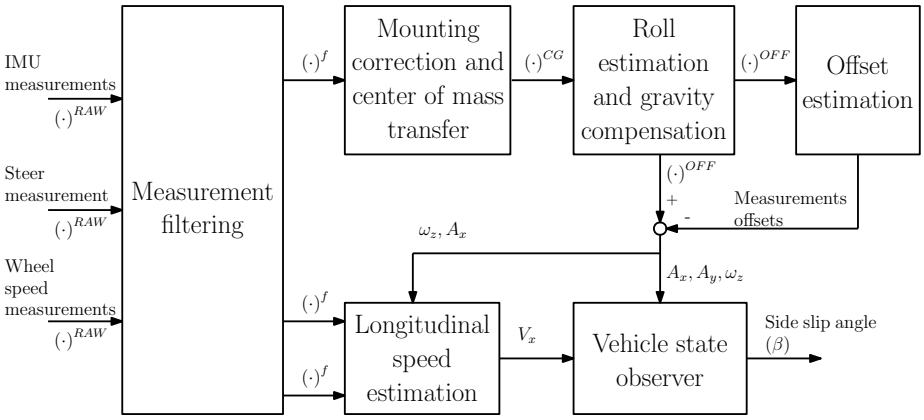

Figure 6: Complete sideslip observer block diagram

3.1. Roll estimation and gravity compensation

The sideslip angle observer requires the vehicle accelerations along its axes. However the vehicle rolls, and gravity acceleration influences the lateral acceleration measurement. To compensate this effect an algorithm for estimating the vehicle roll is introduced. The vehicle rolls as a consequence of the centrifugal force that causes a load transfer between left and right part of the vehicle. The lateral acceleration is a measurement of the centrifugal force, hence a model that relates the vehicle roll to A_y can be written, [41]. Figure 7 shows the vehicle vertical dynamics schematic, where the front and the rear part of the body are considered to have the same behavior. Writing the vertical axis and momentum

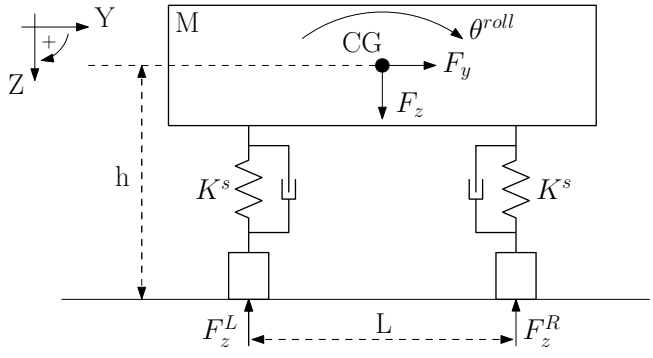

Figure 7: Vertical dynamics schematics

equilibrium one obtains:

$$F_z^L = \frac{F_z^N}{2} - \Delta F_z \qquad F_z^R = \frac{F_z^N}{2} + \Delta F_z \tag{14}$$

$$hF_y - \frac{L}{2}F_z^R + \frac{L}{2}F_z^L = 0 \tag{15}$$

where F_y, F_z^N, F_z^L, F_z^R and ΔF_z are the lateral force, the total vertical force, the vertical force acting on the left wheels, the vertical force acting on the right wheels and the load transfer respectively. Considering that the vehicle lateral force depends on the lateral acceleration ($F_y = MA_y$) and the nominal vertical force is given by gravity acceleration $\left(F_z^N = Mg\right)$, during steady state turning, the following expression relates the roll angle with the lateral acceleration:

$$\theta^{roll} \approx -\frac{Mh}{K^s L^2} A_y \tag{16}$$

where $\frac{Mh}{K^s L^2}$ represents the inverse of the vehicle roll stiffness, M is the vehicle mass and h is the center of mass altitude. Figure 8 shows the measured roll angle and lateral acceleration for different steady state cornering maneuvers. It clearly shows that the steady state roll angle depends on the lateral acceleration and the vehicle roll stiffness.

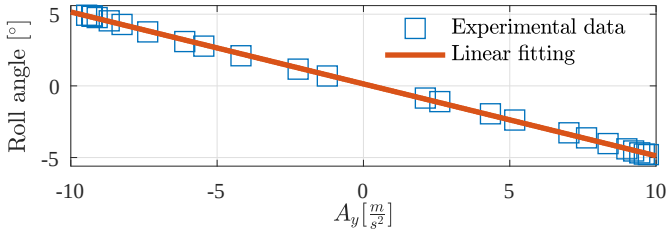

Figure 8: Roll static model vaidation: step steer maneuvers

Equation (16) is a static relation between A_y and the roll angle; it neglects the load transfer dynamics. To improve also the dynamic estimate, the roll rate measurement can be exploited. This is done through a complementary filter. This approach has been derived from [42] where the complementary filter has been used for the estimate of the roll angle in motorcycles. If measurement errors are not present, the roll angle can be obtained by simply integrating the roll rate, however offsets may cause the integral divergence. The complementary filter fuses the high frequency information carried by the roll rate with the static model. Figure 9 shows the schematic of the method. High frequency components of the roll angle are obtained by integrating the high frequency components of the roll rate, and low frequency components are computed by low-pass filtering the static model output.
The estimated roll angle is then used to compensate the measured lateral acceleration according to:

$$A_y^{off} = A_y^{CG} - g \cdot sin\left(\theta^{est}\right). \tag{17}$$

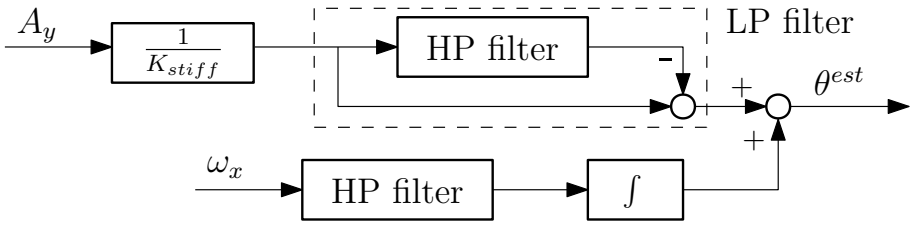

Figure 9: Roll estimation schematic: complementary filter block diagram

A similar method can be used to estimate the pitch angle of the vehicle and compensate the gravity effect on A_x. The pitch angle can be estimated by using a complementary filter to merge the pitch rate measurement with the information of the vehicle pitch static model. However, this is a second order effect which does not directly influence the lateral acceleration and the lateral velocity estimate and can be neglected without affecting the overall performance.

4. Online measurement offset estimation

The state observer is robustly stable with respect to measurement offsets and it can not drift as a result of the heuristic dynamics; yet, an offset estimation algorithm is introduced to improve the estimation performance. The algorithm is based on the frequency separation principle. Offsets are considered slowly varying with respect to other dynamics, hence they are estimated online through low-pass filtering the measurements in properly selected conditions. The low-pass filter used for the gyro offsets has a settling time of 150 s while the acceleration low-pass filters have a settling time of 1500 s. Each offset is managed separately to exploit the properties of the corresponding measurement. They all however behaves according to the same rationale: an activation logic selects the data that satisfy certain properties and activates the low-pass filtering. When the logic is not active the filters are stopped and their state held at the values of deactivation.

Gyros are not affected by gravity; their offsets can be thus estimated during the time period when the vehicle is not moving, regardless of vehicle attitude.

The estimation of the longitudinal offset exploits the estimated longitudinal velocity (V_x). An alternative measurement of the longitudinal acceleration can be obtained by derivation of V_x, properly filtered to remove the high frequency noise. The discrepancy between the measured longitudinal acceleration (A_x^{off}) and V_x derivative ($\frac{dVx}{dt}$) is caused by undesired effects acting on both A_x^{off} and V_x. $\frac{dVx}{dt}$ is influenced by the wheel slips and is not affected by an offset as it is obtained by derivation; A_x^{off} is influenced by the lateral dynamic, the gravity acceleration and the sensor offset. Therefore the offset can be estimated by low-pass filtering the discrepancy between $\frac{dVx}{dt}$ and A_x^{off} in conditions where the lateral dynamics, gravity and slip effects are negligible. The estimation schematic is shown in Figure 10; A_x^{off} is compared with $\frac{dVx}{dt}$, any discrepancy

between the two quantities in the selected conditions is considered a measurement offset. The selected running conditions are the following:

1. vehicle moving conditions ($V_x(t) > 0$);
2. limited longitudinal acceleration conditions ($A_x^{off|<1\frac{m}{s^2}}$): large A_x^{off} causes the vehicle to pitch that in turns leads to a gravity acceleration component on the longitudinal acceleration. Moreover large A_x^{off} correspond to large wheel slips;
3. straight moving conditions $\omega_z(t) \leq 5\frac{^\circ}{s}$): on cornering A_x^{off} is influenced by lateral dynamics.

Selected samples are then filtered through a low-pass filter.

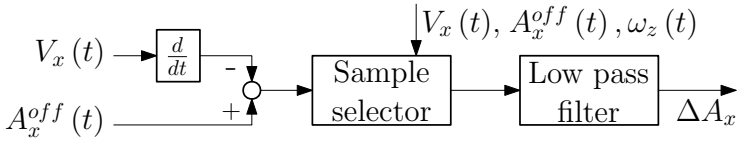

Figure 10: Longitudinal acceleration (A_x) offset estimation block diagram

The lateral acceleration offset estimation takes advantage of the kinematic model combined with the A_y sensor output model. The processed sensor output ($A_y^{off}(t)$) is considered to be a combination of the real vehicle lateral acceleration (A_y), the time varying sensor offset (ΔA_y) and a zero mean white noise ($\epsilon_y(t)$).

$$\begin{cases} \dot{V}_y(t) = A_y(t) - \omega_z(t) V_x(t) \\ A_y^{off}(t) = A_y(t) + \Delta A_y(t) + \epsilon_y(t) \end{cases} \tag{18}$$

Combining the two equations of (18) one obtains an expression of the sensor offset:

$$\Delta A_y(t) = A_y^{off}(t) - \omega_z(t) V_x(t) - \dot{V}_y(t) - \epsilon_y(t). \tag{19}$$

Since the problem of offset estimation concerns slow varying dynamics, only mean values of the quantities in (19) are considered. $\epsilon_y(t)$ has zero mean by definition, while $\dot{V}_y$ mean value requires a more detailed analysis. The mean value of the derivative of the lateral velocity on a certain time interval can be related to the vehicle lateral velocity with the following:

$$E\left[\dot{V}_y(t)\right] = \frac{1}{t_f - t_0} \int_{t_0}^{t_f} \dot{V}_y(t)\, dt = \frac{V_y(t_f) - V_y(t_0)}{t_f - t_0}, \tag{20}$$

for a generic route, starting and finishing with a straight movement, the derivative of the lateral velocity is zero on average $\left(E\left[\dot{V}_y(t)\right] \approx 0\right)$ and it can be ignored for the offset estimation goal. At the end an expression for A_y offset estimation is given by:

$$\Delta A_y(t) = A_y^{off}(t) - \omega_z(t) V_x(t). \tag{21}$$

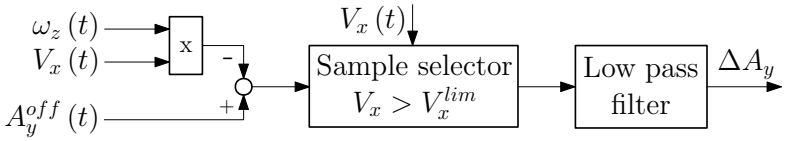

Figure 11: Lateral acceleration (A_y) offset estimation block diagram

Figure 11 shows the estimation schematic and, as for the previous cases data are filtered by a low-pass filter. If the vehicle runs constantly on a slant or banked road the methods estimate the sum of the sensor offset and the constants component of the gravity acceleration. This behavior is correct, as the goal is the sideslip estimation.

5. Experimental results

This section experimentally validates the estimation approach. All the experiments are performed on an instrumented Alfa Romeo 159 with a nominal mass of 1875 Kg, a 2.4 L engine with all wheel drive. The vehicle is equipped with an automotive certified solid state 6 DoF inertial measurement unit (IMU), wheels speed measurements, steer angle measurement and optical sideslip angle measurement. Two different set-ups are used to evaluate the method performance:

1. Roll estimate set-up: to evaluate the algorithm introduced in Section 3.1 a specific set-up for the measurement of the roll angle is needed. A three-point laser measurement system provides the distances from ground of three corners and the vehicle roll angle is obtained through straightforward geometrical considerations.
2. Sideslip angle set-up: for the evaluation of the other estimation algorithms introduced here, the vehicle is equipped with an optical system for the measurement of the vehicle velocity with respect to the ground.

Except for roll angle and optical sideslip angle measurements, all other quantities are measured by series production off-the-shelf sensors.

A total of seven tests will be shown. One test is used for the validation of the roll angle estimate, one is used for the validation of the measurements offset estimation and the rest are used for the sideslip angle validation in various conditions. Sideslip angle validation is done on high adherence surface (high and low sideslip maneuvers) and low adherence surface. For all the tests the vehicle is equipped with different controllers acting on the lateral dynamics and longitudinal dynamics. The sideslip estimation has no information on these controllers.

The method depends on different tuning parameters. The longitudinal velocity method relies upon the $A_x^{threshold}$, σ_{w1} and σ_{w2}; the parameters are tuned by minimizing the RMS of the longitudinal velocity error. The sideslip estimation parameters, the closed loop observer parameters (α_0,α_1,α_2) and the heuristic

functions, are tuned by minimizing the RMS of the sideslip angle error. The tuning is done on all the available data in order to obtain a single set of parameters used for all the experimental tests. The values of the parameters used for the results of this Section are provided in Table 1.

Table 1: Tuning parameter values

Parameter	Value	Parameter	Value
α_0	10	α_1	5
α_2	10	$A_x^{threshold}$	$1\frac{m}{s^2}$
$\sigma_{d\omega_1}$	4.5	$\sigma_{d\omega_2}$	1
σ_{ω_z}	0.18	$\sigma_{d\omega_z}$	0.18
σ_δ	0.1	$\sigma_{d\delta}$	0.1
$\sigma_{\dot{\beta}}$	0.06	$\sigma_{d\dot{\beta}}$	0.3

5.1. Roll angle estimation

Figure 12 presents the results of the roll angle estimate. The algorithm performs well for all maneuvers. It presents a maximum estimate error of 0.6°. The latter corresponds to an error of 0.1m/s^2 on the lateral acceleration which is negligible compared to the vehicle acceleration. The average of the estimate error is 0 and its RMS value is 0.12°.

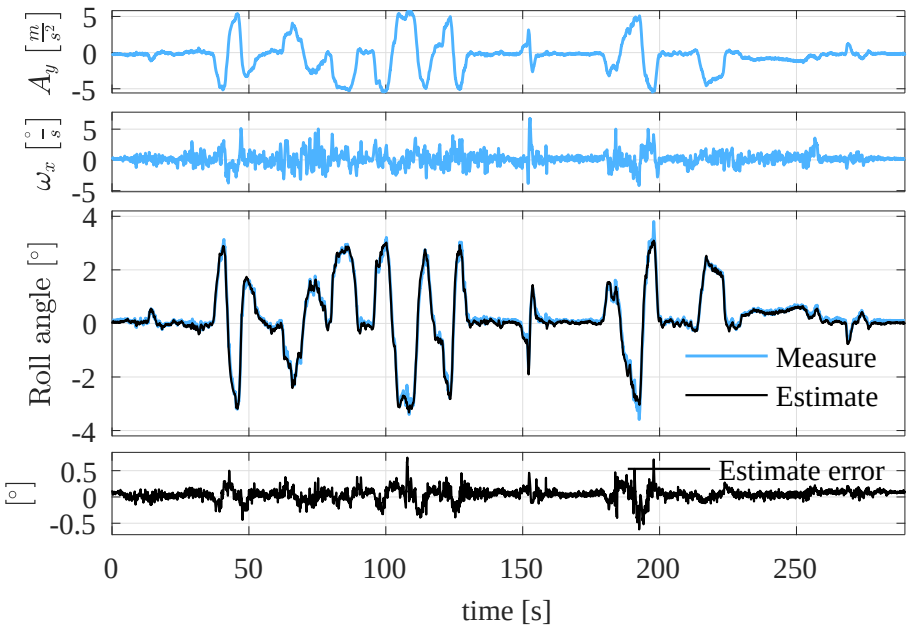

Figure 12: Roll estimatimation results: RMS(Estimate error)=0.12°

5.2. Offset estimation results

The offset estimation validation requires a long test because of the inherently slow dynamics of the offset. To better assess the convergence of the algorithm, the estimation has been initialized to purposely large offset. In reality, the algorithm is always initialized at the most recent estimation at every key-on of the vehicle.

Figure 13 plots the results in terms of offset estimation on a road with varying adherence; the figure compares the estimate against the true offset estimated offline. The gyro offset estimation is straightforward; the estimate converges to the offset during the vehicle stops and is insensitive to measurement noise. A_x and A_y offset estimation is more critical as the acceleration measurements are influenced by road banking. From $t = 2000$ s to $t = 2500$ s, the vehicle runs on the parabolic curve track and the algorithm tends to estimate the gravity component influencing the measures together with the sensor offset. Two considerations are due: (i) if the vehicle is permanently running on a banked road then it is correct to consider the gravity effect as a measurement offset, since the objective is that of estimating the sideslip angle with respect to the road plane; (ii) on long driving tests the road banking can be considered as a zero average effect, in fact after a transient phase the estimated offset converges to the real sensor offset.

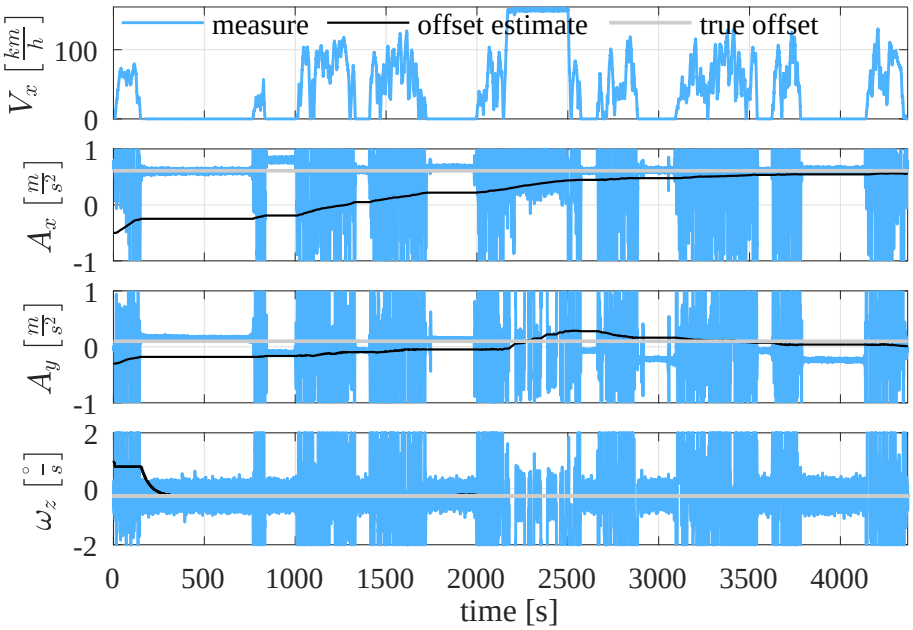

Figure 13: Offset estimation experimental results

5.3. Step steer maneuver

The step steer maneuver is an objective test. The limited impact of the driver driving style allows for a good repeatability. The maneuver consists of a steer step of 7° while the speed is kept constant. Figure 14 shows the inertial measurements (corrected and transferred to the center of mass). The longitudinal acceleration is nearly zero while the lateral acceleration and the yaw rate reach 9 m/s^2 and 25°/s respectively. This maneuver evaluates the best performance of the method for low sideslip angle conditions as no road bank/slope is present. The estimation results are shown in Figure 15; the algorithm performs well with an RMS of the estimate error of 0.48° and a maximum estimation error of 1°.

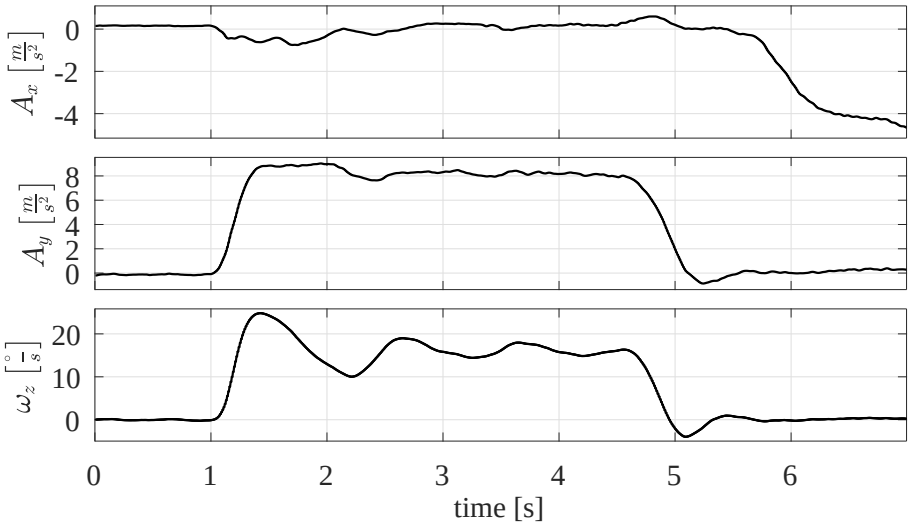

Figure 14: Step steer test: vehicle inertial measurements

5.4. High μ test

High friction roads represent the majority of road conditions where commercial vehicles are used. Two tracks, both with $\mu \approx 1$, are tested; one track is used to evaluate the method performances on city driving (*i.e.*, driving characterized by low sideslip maneuvers) while the other is used for sporty driving (*i.e.*, driving characterized by large sideslip maneuvers).

The first track is characterized by two long straight paths, a smooth and long curve and different sharp and fast curves. The vehicle speed experiences time intervals with small variations during the curves and time intervals with large variation during straight driving. Figure 16 and 17 show respectively the inertial measurements and the longitudinal velocity estimation which is compared with the measured velocity and the average of the wheel velocities. A_x presents relevant peaks during the braking maneuvers; a clear example is the maneuver

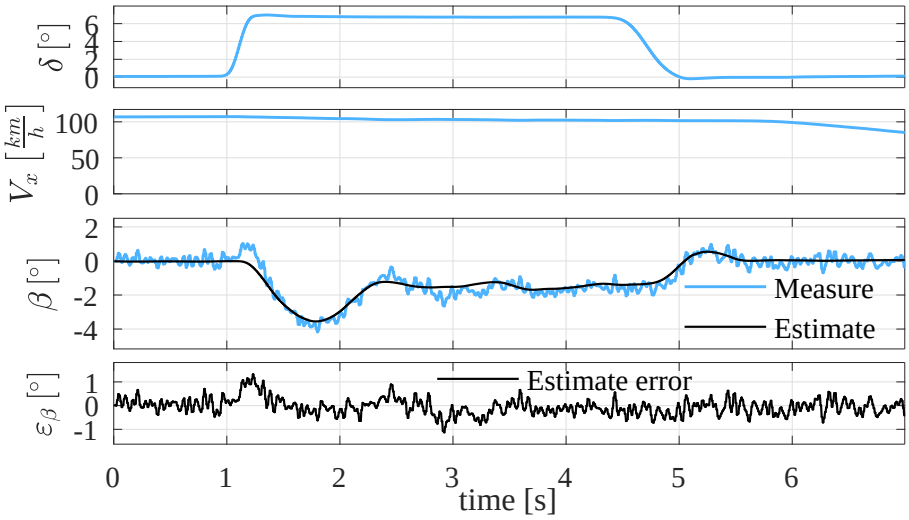

Figure 15: Step steer test: side slip estimate. RMS(ε_β)=0.48°

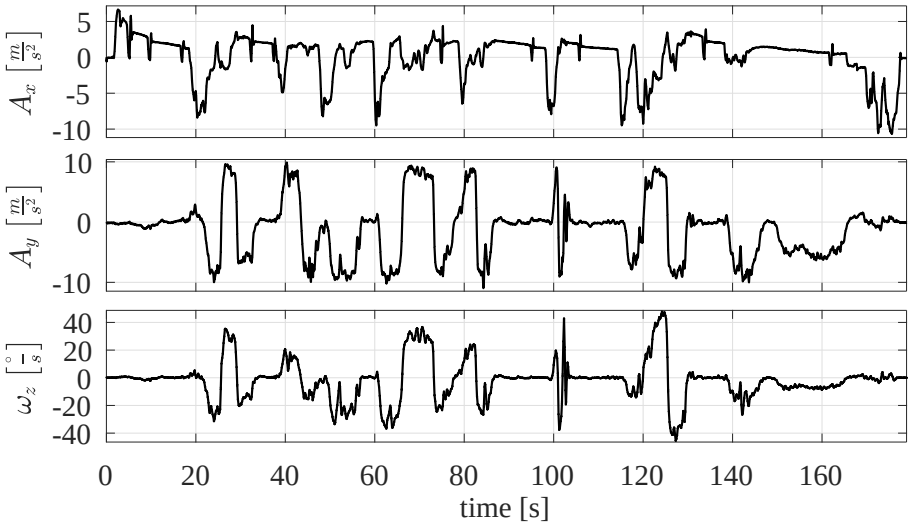

Figure 16: High adherence low sideslip test: vehicle inertial measurements

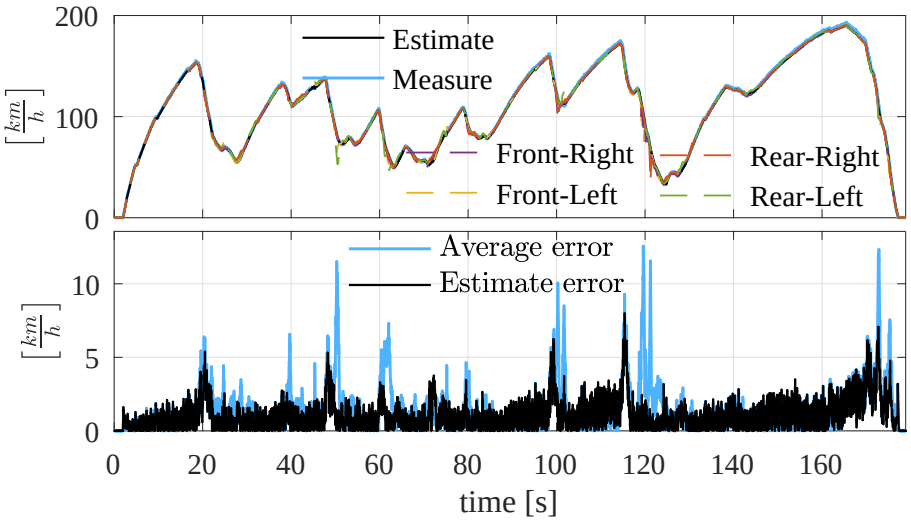

Figure 17: High adherence low sideslip test: longitudinal speed estimate. The average error is the difference between the measured speed and the wheel velocities average; RMS(average error)=2.09 km/h. The estimate error is is the difference between the measured speed and the speed estimated by the proposed method; RMS(estimate error)=1.41 km/h.

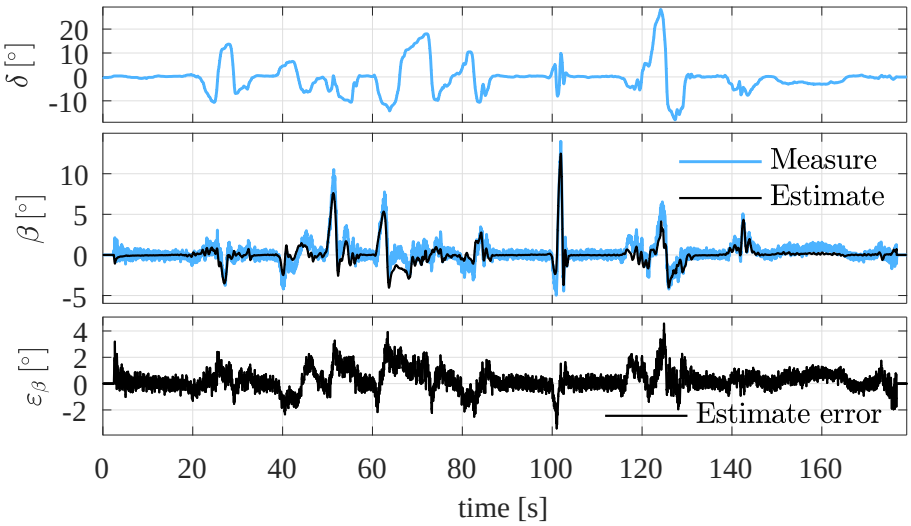

Figure 18: High adherence low sideslip test: sideslip estimate. RMS(ε_β)=0.85°

at t≈ 120 s, immediately before starting a curve. The driver performs a sharp braking maneuver and enters the curve; in this condition estimations based on wheel velocities lose reliability and the introduced algorithm outperforms the average speed (computed as $\frac{1}{4}\sum_i V_i$), both in the error RMS sense and maximum error sense. The lateral acceleration and the yaw rate (Figure 16) are small during straight and nearly straight drivings (t< 20 s, 90 s<t<100 s, 105 s<t<115 s, t>160 s). During curves A_y and ω_z reach large values, respectively 10 m/s^2 and 50°/s. In all conditions, the observer performs well; although the sideslip estimation (Figure 18) deteriorates compared to the step steer case, the error RMS is 0.85°. The main reasons for this deterioration are:

1. rapid variations of road banking and slope;
2. severe acceleration that cause high wheels longitudinal slip and deteriorates the longitudinal speed estimation;
3. vehicle pitch caused by strong acceleration that is not taken into consideration.

The results also show the main advantage of the heuristic dynamics, during straight maneuvers the estimated sideslip angle is zero. The method is robust to any measurement error or gravity effect and does not present drift. Executing the observer on the same maneuver, but with weaker heuristic correction term the results of Figure 19 are obtained. Without the heuristic the performance of the observer considerably deteriorates. During strong turning maneuvers (98 s<t<105 s) the observer without heuristic can estimate the sharp variations of the sideslip angle, since the kinematic model is observable. However, during straight maneuvers (t>140 s) the estimation tends to diverge as the kinematic model loses its observability for $\omega_z \approx 0$.

The second track is used to test the method during aggressive driving that reaches high sideslip angle. The inertial measurement evolution (Figure 20) reflects the track characteristics; since the track is mostly composed of curves, A_y and ω_z are nearly zero only for a limited number of short time intervals (t<15 s, 40 s<t<45 s, 74 s<t<82 s, 210 s<t<214 s, t>265 s). A_x presents sharp variations as the driver brakes and accelerates brusquely while entering and exiting the curves. The vehicle speed estimation and the wheel speeds are shown in Figure 21. During sharp accelerations, such as 55 s<t<75 s and 190 s<t<200 s, the rear wheels tend to diverge since the vehicle is a rear wheel drive. In these conditions, the V_x estimation algorithm presents the major advantages; it discards the diverging wheel limitng the estimation error. The sideslip angle estimation results are shown in Figure 22. The test presents high β, low β as well as straight maneuvers. In all conditions the estimation performs well; the estimation error maximum value and RMS are similar to the low β condition.

5.5. Low μ test

The fourth test that is considered is a low adherence test track ($\mu \approx 0.3$). The track is composed of one straight path followed by soft curves. During this test, the vehicle reaches high sideslip angle in most maneuvers. However,

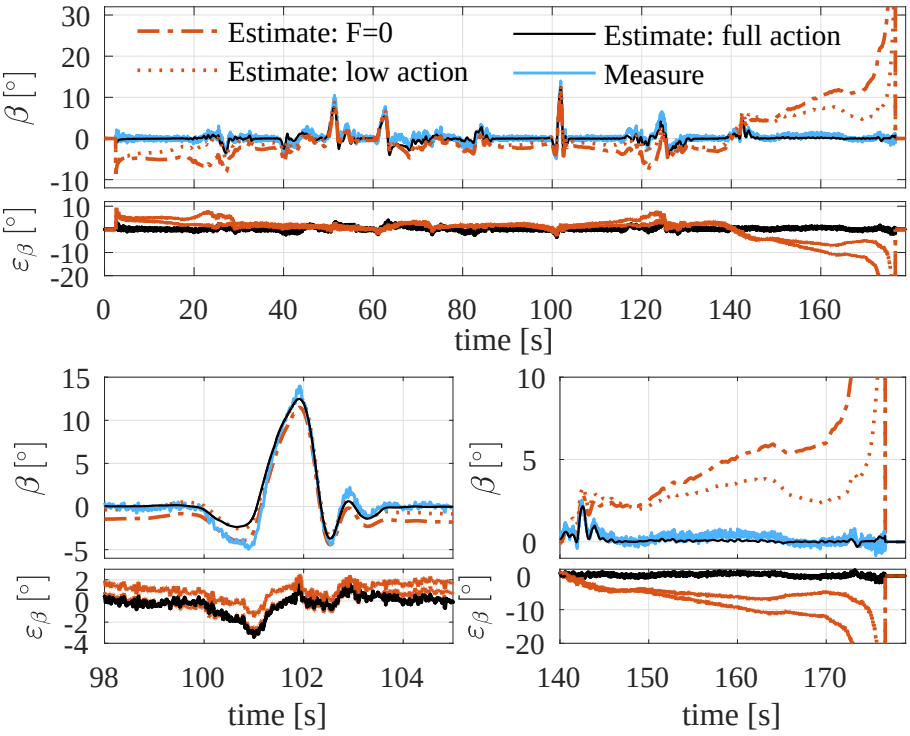

Figure 19: Heuristic effect

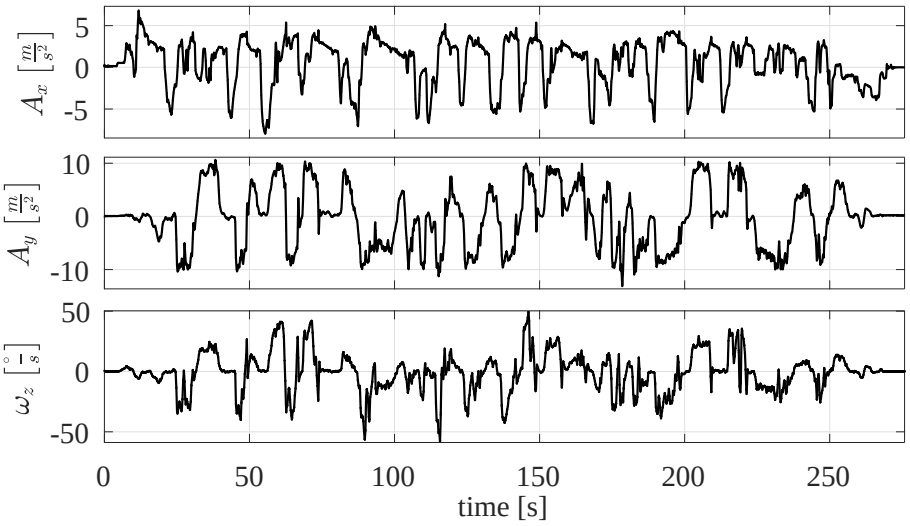

Figure 20: High adherence high sideslip test: vehicle inertial measurements

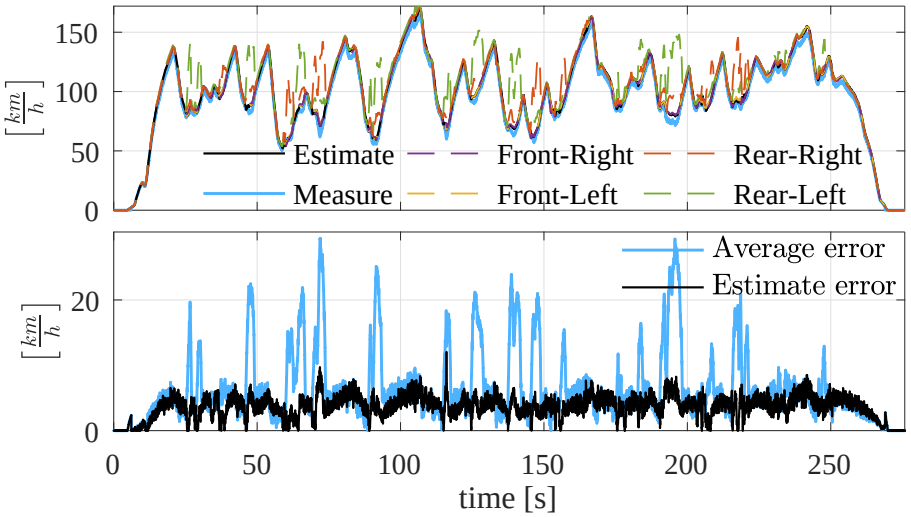

Figure 21: High adherence high sideslip test: longitudinal speed estimate. RMS(average error)=8.36km/h, RMS(estimate error)=4.01km/h.

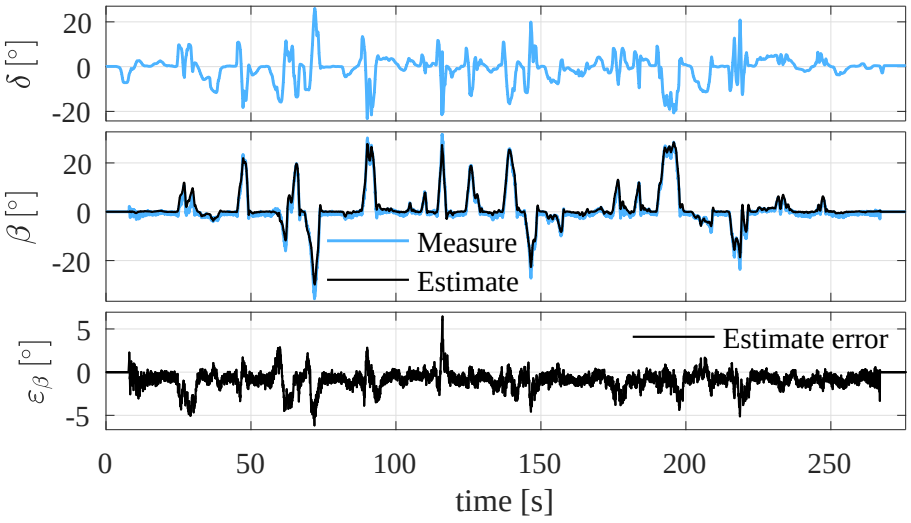

Figure 22: High adherence high sideslip test: sideslip estimate. RMS(ε_β)=1°

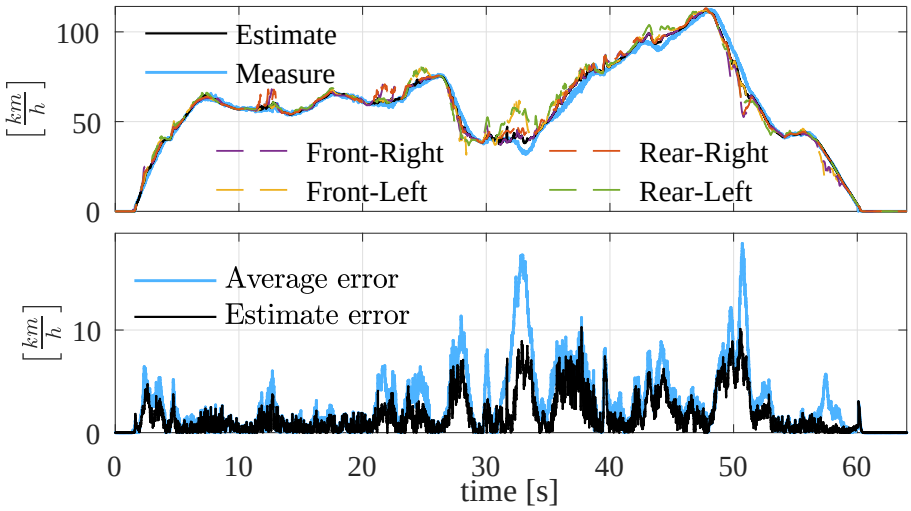

Figure 23: Low adherence test: longitudinal speed estimate. RMS(average error)=4.24km/h, RMS(estimate error)=2.45km/h.

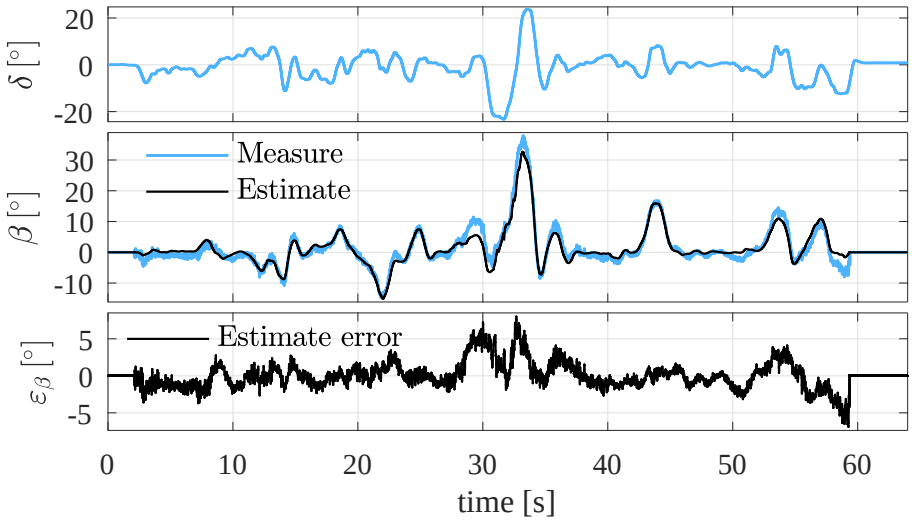

Figure 24: Low adherence test: side slip estimate. RMS(ε_β)=1.10°

measured accelerations present lower values compared to the high adherence track. The low grip influences also the wheel velocities behavior (Figure 23), with lower grip the velocities are noisier despite the low longitudinal acceleration (30 s<t< 45 s).

Although the driving and road conditions are severe the observer works correctly and preserves an estimation error comparable with the previous tests (RMS value of 1.10°). In particular the maneuver at time 30 s <t< 37 s shows that at low grip and large β the method preserves its accuracy and presents absolute errors similar to the maneuvers at high grip and small β (Figure 18).

To further validate the accuracy and robustness of the method, the accuracy indexes are computed on a 4000 s test. The sideslip estimation presents a RMS(ε_β) of 0.78° and a maximum error of 6.73°.

6. Robustness analysis

The main advantage of the kinematic approach is its independence from the vehicle parameters, which can be difficult to estimate and can vary. The core of the proposed method is unaffected by vehicle parameters. However, in order to obtain the vehicle center of mass accelerations, the IMU position has to be known and the roll angle estimation needs the roll stiffness. While the IMU position is constant during the use of the vehicle, the roll stiffness depends on the vehicle mass. The following tests highlight the performance of the method in non nominal conditions and on data that were not used during the tuning phase.

The effect of the vehicle mass on the sideslip angle estimate is analyzed by testing the method on a steer step maneuver and the vehicle loaded with additional 300 Kg. The accelerations measured during the test are similar to the step steer test with nominal load. The vehicle speed is nearly constant, hence the measured A_x is nearly zero. The lateral acceleration and the yaw rate reach 9m/s^2 and 25°/s respectively and demonstrate the severity of the maneuver. β estimation results in Figure 25 show the robustness of the method to vehicle mass, as the estimation error presents negligible differences with the nominal load case.

An additional test is performed on a mix high and low adherence track, Figure 26. The first part corresponds to the high adherence track used for the test of Figure 18 and the second part corresponds to a track with a friction coefficient of approximately 0.2. For both parts the method uses the same parameters and has no information on the friction. The overall performance deteriorate compared to high friction test. However, the method is designed to estimate fast sideslip variations on unknown road characteristics and to this end the results are satisfactory.

As described, the core vehicle state observer is sided by a number of additional terms and correction. Each term improves the performance under specific conditions. It is therefore useful to try and quantitatively assess the contribution of each term. Table 2 summarizes the relative loss of accuracy when the

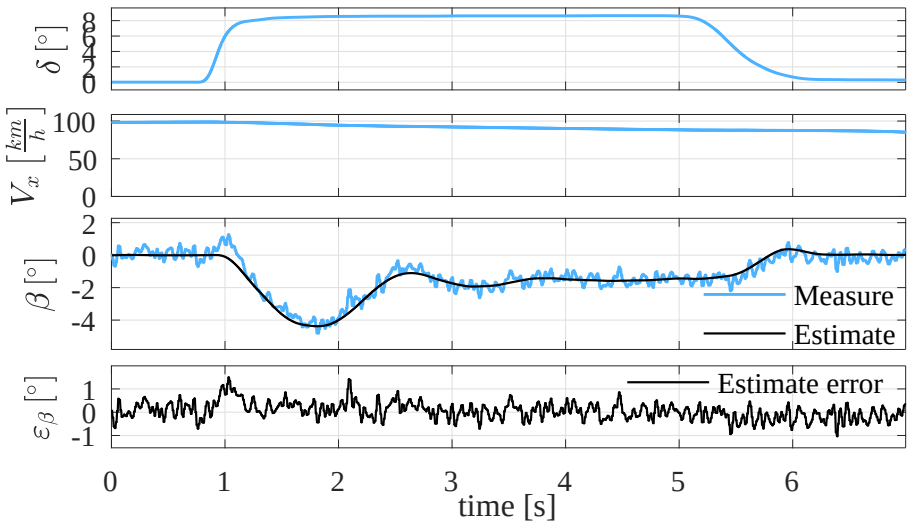

Figure 25: Step steer test with loaded vehicle. RMS(estimate error)=0.50°

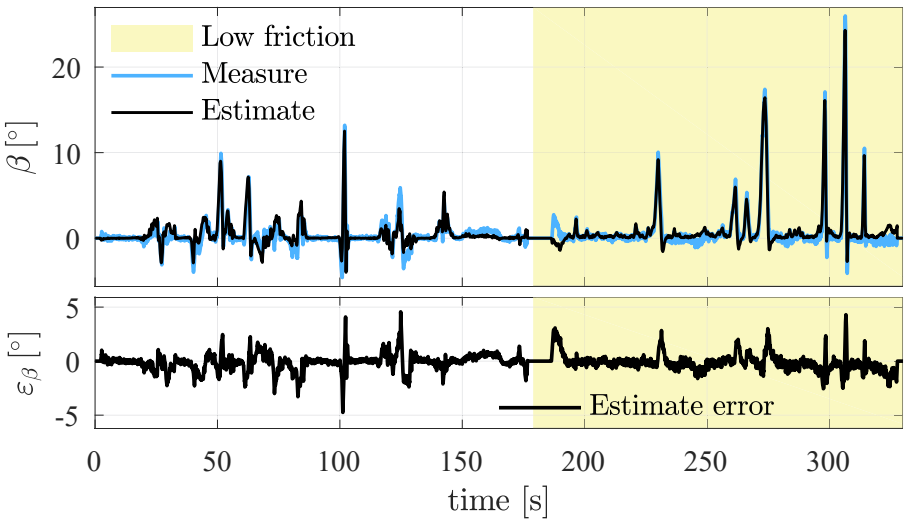

Figure 26: High and low grip combined test. RMS(estimate error)=0.96°. Note the sharp increase of the sideslip estimation error at around 180 s. At that time, the rider performs a sudden acceleration from a standing still; at such low speed (v¡20km/h), also the optical sensor is subject to measurement errors.

different blocks are selectively disabled in the high grip, low β scenario. The estimation algorithm is run on the same data disabling a single correction term at the time. All blocks play an important role in the reduction of the estimation error, some of them have a prevalent impact on the maximum error, some of them on the overall RMS performance. Generally speaking, the blocks that aim at correcting the lateral acceleration (namely A_y offset computation, and roll estimation) are the most important. The center of mass translation is important especially during sharp maneuvers when the crosstalk between different axes is the strongest, and thus it mainly affects the maximum error. For similar reasons, the speed estimation algorithm mainly impacts the maximum error as it intervenes more heavily during aggressive maneuvers.

Table 2: Summary of the effect of additional blocks

Disabled block	Δ **MAX**(ε_β)	Δ **RMS**(ε_β)
A_x Offset est.	4%	1%
A_y Offset est.	14%	22%
ω_z Offset est.	7%	24%
Center of mass translation	74%	8%
Roll estimation	37%	30%
Speed estimation	28%	1%

7. Conclusions

This paper discusses a complete, robust and industrially viable method for estimating sideslip angle in cars making use of low-cost off-the-shelf sensors, such as body accelerometers, rate gyros, wheel velocities and steering wheel angle.

The algorithm is composed of different components estimating the vehicle longitudinal speed, the sensor offsets, the vehicle roll angle and the center of mass accelerations. All the components exploit kinematic considerations and are designed to be independent from the vehicle parameters and road conditions. These algorithms are used to process the measured accelerations and angular rates in order to obtain the center of mass quantities.

The observer combines the vehicle kinematic model, that is unaffected by the vehicle parameters, and a heuristic term that adds experience-based information. Compared with previous solutions presented in literature the method presents two main advantages:

1. being based on the kinematic model the method is unaffected by vehicle parameters and tire-road friction. All the methods relying on a grip model require an online estimate of the grip in order to work properly, which is possible only if excited driving maneuvers are executed;
2. the heuristic term ensures a correct behavior also during straight driving. Methods relying purely on the kinematic model present a critical behavior

on straight driving; the kinematic model becomes unobservable and the estimate tends to diverge due to measurement offsets.

The method is tested on a vast collection of trials: step steer maneuver, high grip track and low β conditions, high grip track and high β conditions and low grip track. The paper discusses at length the features of the algorithm for each test. The results of the algorithm can be summarized in Figure 27 that summarizes the estimation error statistics in different conditions. The estimation results are satisfactory ($\max_{RMS}$=1.1°) although the method does not have any information about the grip condition. Finally, the estimation methods are computationally efficient and are implemented on a production electronic control unit.

References

[1] G. Leen, D. Heffernan, Expanding automotive electronic systems, Computer 35 (1) (2002) 88–93.

[2] A. T. Van Zanten, Evolution of electronic control systems for improving the vehicle dynamic behavior, in: Proc. Int. Symp. on Advanced Veh. Control (AVEC), 2002, pp. 1–9.

[3] D. Piyabongkarn, J. Y. Lew, R. Rajamani, J. A. Grogg, Q. Yuan, On the use of torque-biasing systems for electronic stability control: limitations and possibilities, IEEE Trans. Control Syst. Technol. 15 (3) (2007) 581–589.

[4] L. Laine, J. Andreasson, Control allocation based electronic stability control system for a conventional road vehicle, in: IEEE Intell. Transp. Syst. Conf. (ITSC), IEEE, 2007, pp. 514–521.

[5] R. Marino, S. Scalzi, F. Cinili, Nonlinear pi front and rear steering control in four wheel steering vehicles, Veh. Syst. Dynamics 45 (12) (2007) 1149–1168.

[6] D. Selmanaj, M. Corno, O. Sename, S. Savaresi, Advantages of rear steer in lti and lpv vehicle stability control, in: Proc. Conf. on Decision and Control (CDC), IEEE, 2013, pp. 3523–3528.

[7] K. Koibuchi, M. Yamamoto, Y. Fukada, S. Inagaki, Vehicle stability control in limit cornering by active brake, in: SAE Technical Paper, SAE International, 1996. doi:10.4271/960487.

[8] J. He, D. A. Crolla, M. Levesley, W. Manning, Coordination of active steering, driveline, and braking for integrated vehicle dynamics control, Proc. Institution of Mechanical Engineers, Part D: Journal of Automobile Eng. 220 (10) (2006) 1401–1420. doi:10.1243/09544070JAUTO265.

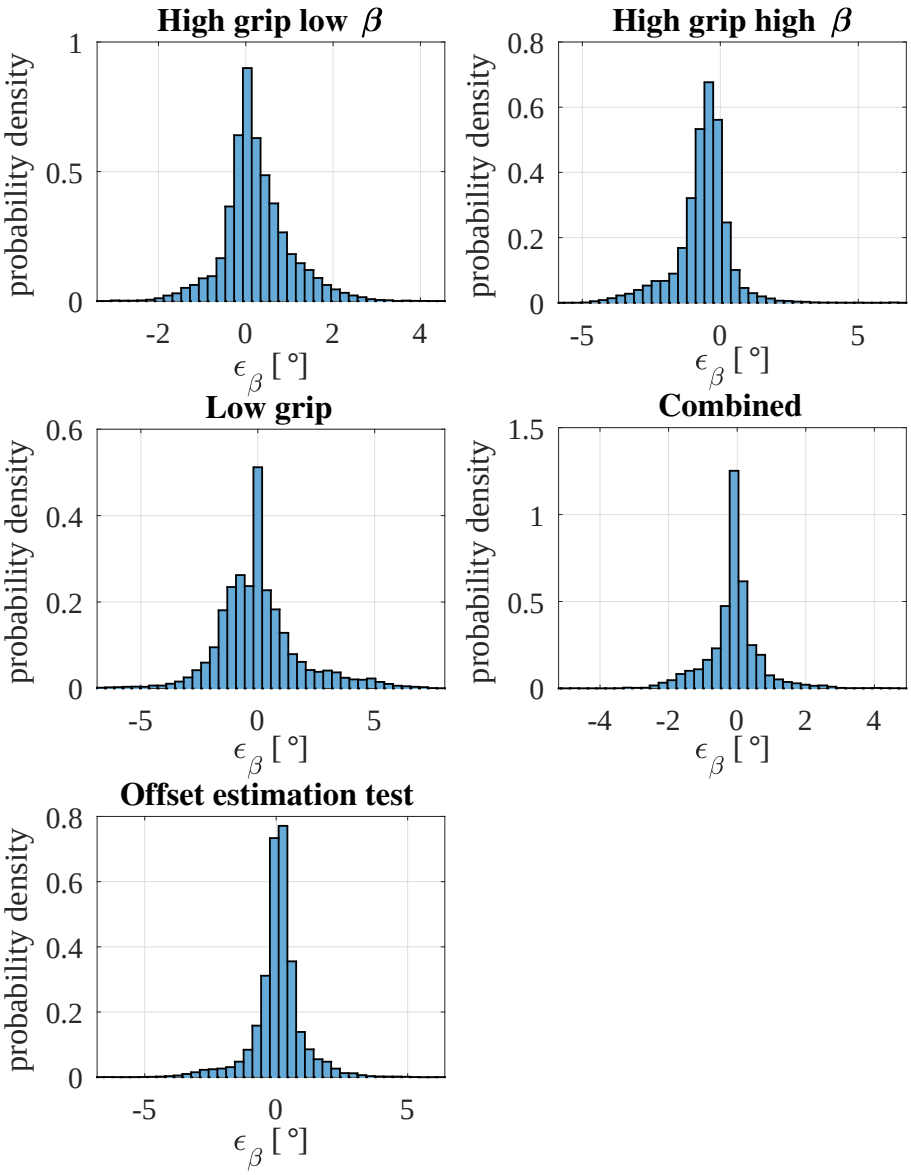

Figure 27: Distribution of the estimation error.

[9] J. Ryu, E. J. Rossetter, J. C. Gerdes, Vehicle sideslip and roll parameter estimation using gps, in: Proc. Int. Symp. on Advanced Veh. Control (AVEC), Vol. 2, 2002, pp. 373–380.

[10] X. Li, C. Chan, Y. Wang, A reliable fusion methodology for simultaneous estimation of vehicle sideslip and yaw angles, IEEE Trans. Veh. Technol. 65 (6) (2016) 4440–4458. doi:10.1109/TVT.2015.2496969.

[11] J.-H. Yoon, H. Peng, A cost-effective sideslip estimation method using velocity measurements from two gps receivers, IEEE Trans. Veh. Technol. 63 (6) (2014) 2589–2599. doi:10.1109/TVT.2013.2294717.

[12] D. M. Bevly, J. C. Gerdes, C. Wilson, The use of gps based velocity measurements for measurement of sideslip and wheel slip, Veh. Syst. Dynamics 38 (2) (2002) 127–147.

[13] D. M. Bevly, J. Ryu, J. C. Gerdes, Integrating ins sensors with gps measurements for continuous estimation of vehicle sideslip, roll, and tire cornering stiffness, IEEE Trans. Intell. Transp. Syst. 7 (4) (2006) 483–493.

[14] J. H. Yoon, H. Peng, Robust vehicle sideslip angle estimation through a disturbance rejection filter that integrates a magnetometer with gps, IEEE Trans. Intell. Transp. Syst. 15 (1) (2014) 191–204. doi:10.1109/TITS.2013.2275173.

[15] K. Nam, H. Fujimoto, Y. Hori, Lateral stability control of in-wheel-motor-driven electric vehicles based on sideslip angle estimation using lateral tire force sensors, IEEE Trans. Veh. Technol. 61 (5) (2012) 1972–1985. doi:10.1109/TVT.2012.2191627.

[16] A. K. Madhusudhanan, M. Corno, E. Holweg, Vehicle sideslip estimator using load sensing bearings, Control Engineering Practice 54 (2016) 46–57.

[17] A. Kunnappillil Madhusudhanan, M. Corno, E. Holweg, Sliding mode-based lateral vehicle dynamics control using tyre force measurements, Vehicle System Dynamics 53 (11) (2015) 1599–1619.

[18] M. Corno, M. Gerard, M. Verhaegen, E. Holweg, Hybrid abs control using force measurement, IEEE Transactions on Control Systems Technology 20 (5) (2012) 1223–1235.

[19] H. Sasaki, T. Nishimaki, A side-slip angle estimation using neural network for a wheeled vehicle, in: SAE Technical Paper, SAE International, 2000. doi:10.4271/2000-01-0695.
URL http://dx.doi.org/10.4271/2000-01-0695

[20] M. Milanese, D. Regruto, A. Fortina, Direct virtual sensor (dvs) design in vehicle sideslip angle estimation, in: Proc. American Control Conf. (ACC), IEEE, 2007, pp. 3654–3658.

[21] J. Stephant, A. Charara, D. Meizel, Evaluation of a sliding mode observer for vehicle sideslip angle, Control Engineering Practice 15 (7) (2007) 803–812.

[22] G. Baffet, A. Charara, D. Lechner, Estimation of vehicle sideslip, tire force and wheel cornering stiffness, Control Engineering Practice 17 (11) (2009) 1255–1264.

[23] T. A. Wenzel, K. Burnham, M. Blundell, R. Williams, Dual extended kalman filter for vehicle state and parameter estimation, Veh. Syst. Dynamics 44 (2) (2006) 153–171.

[24] J. L. Coyte, B. Li, H. Du, W. Li, D. Stirling, M. Ros, Decision tree assisted ekf for vehicle slip angle estimation using inertial motion sensors, in: Proc. Int. Joint Conf. on Neural Netw. (IJCNN), IEEE, 2014, pp. 940–946.

[25] J. Dakhlallah, S. Glaser, S. Mammar, Y. Sebsadji, Tire-road forces estimation using extended kalman filter and sideslip angle evaluation, in: Proc. American Control Conf. (ACC), IEEE, 2008, pp. 4597–4602.

[26] J. Farrelly, P. Wellstead, Estimation of vehicle lateral velocity, in: Proc. IEEE Int. Control App. Conf., IEEE, 1996, pp. 552–557.

[27] G. Panzani, M. Corno, M. Tanelli, A. Zappavigna, S. M. Savaresi, A. Fortina, S. Campo, Designing on-demand four-wheel-drive vehicles via active control of the central transfer case, IEEE Trans. Intell. Transp. Syst. 11 (4) (2010) 931–941. doi:10.1109/TITS.2010.2055858.

[28] H. Kim, J. Ryu, Sideslip angle estimation considering short-duration longitudinal velocity variation, Int. Journal of Automotive Technology 12 (4) (2011) 545–553.

[29] L. Wei, L. Wenying, D. Haitao, G. Konghui, Side-slip angle estimation for vehicle electronic stability control based on sliding mode observer, in: Proc. Int. Conf. on Measurement, Information and Control (MIC), Vol. 2, IEEE, 2012, pp. 992–995.

[30] F. Cheli, E. Sabbioni, M. Pesce, S. Melzi, A methodology for vehicle sideslip angle identification: comparison with experimental data, Veh. Syst. Dynamics 45 (6) (2007) 549–563.

[31] Y. Fukada, Slip-angle estimation for vehicle stability control, Veh. Syst. Dynamics 32 (4-5) (1999) 375–388.

[32] J. J. Oh, S. B. Choi, Vehicle velocity observer design using 6-d imu and multiple-observer approach, IEEE Trans. Intell. Transp. Syst. 13 (4) (2012) 1865–1879.

[33] D. Piyabongkarn, R. Rajamani, J. A. Grogg, J. Y. Lew, Development and experimental evaluation of a slip angle estimator for vehicle stability control, IEEE Trans. Control Syst. Technol. 17 (1) (2009) 78–88.

[34] H. F. Grip, L. Imsland, T. A. Johansen, T. I. Fossen, J. C. Kalkkuhl, A. Suissa, Nonlinear vehicle side-slip estimation with friction adaptation, Automatica 44 (3) (2008) 611–622.

[35] L. Imsland, H. F. Grip, T. A. Johansen, T. I. Fossen, J. C. Kalkkuhl, A. Suissa, Nonlinear observer for vehicle velocity with friction and road bank angle adaptation-validation and comparison with an extended kalman filter, Tech. rep., SAE Technical Paper (2007).

[36] H. F. Grip, L. Imsland, T. A. Johansen, J. C. Kalkkuhl, A. Suissa, Vehicle sideslip estimation, IEEE Control. Syst. Mag. 29 (5) (2009) 36–52.

[37] S. Han, K. Huh, Monitoring system design for lateral vehicle motion, IEEE Trans. Veh. Technol. 60 (4) (2011) 1394–1403. doi:10.1109/TVT.2011.2122312.

[38] D. Selmanaj, M. Corno, S. M. Savaresi, G. Panzani, G. Bussalai, C. Girardin, Method for estimating a vehicle side slip angle, computer program implementing said method, control unit having said computer program loaded, and vehicle comprising said control unit, Tech. Rep. WO2016062327 (2016).

[39] S. M. Savaresi, M. Tanelli, Active braking control systems design for vehicles, Springer Science & Business Media, 2010.

[40] M. Klomp, Y. Gao, F. Bruzelius, Longitudinal velocity and road slope estimation in hybrid electric vehicles employing early detection of excessive wheel slip, Veh. Syst. Dynamics 52 (sup1) (2014) 172–188.

[41] T. Gillespie, Fundamentals of Vehicle Dynamics, Society of Automotive Engineers, 1992.
URL https://books.google.it/books?id=L6xd0nx5KbwC

[42] I. Boniolo, S. Savaresi, M. Tanelli, Roll angle estimation in two-wheeled vehicles, Control Theory & Applications, IET 3 (1) (2009) 20–32.